Bonding state of silicon segregated to α-iron surfaces and on iron silicide surfaces studied by electron spectroscopy

B. Egert and G. Panzner
Max-Planck-Institut für Eisenforschung, D-4000 Düsseldorf 1, Federal Republic of Germany
(Received 8 April 1983; revised manuscript received 15 June 1983)

Combined (x-ray, ultraviolet) photoelectron, electron- and bremsstrahlung-excited Auger-electron, and electron-energy-loss (EELS) spectroscopic investigations yield insight into the bonding state of silicon (i) as segregated onto Fe(100) forming a $c(2\times2)$ superstructure at equilibrium, and (ii) on Fe_3Si(100), FeSi(100), and $FeSi_2$(poly) surfaces. The slight binding-energy shifts of the Si 2*s*, Si 2*p*, and Fe 3*p* core levels as compared with the pure elements (α-iron and silicon) indicate a small charge transfer from iron to silicon atoms in the silicides. For silicon in the segregated state, the bonding exhibits a predominantly homopolar character. The iron silicide valence bands show an invariable nonbonding Fe 3*d*–derived feature and bonding iron states about 2 eV below E_F. Independent of the Si bulk content, the density of states near E_F is always high, reflecting the intermetallic character of the iron-silicon compounds. The Si- and Fe-induced valence states and interatomic features in the Si($L_{23}VV$) Auger transitions are evidence of the prevailing iron-silicon interaction in Fe_3Si and localized silicon bonding in the monosilicide and disilicide. Segregated Si on Fe(100) at surface saturation interacts for the most part laterally, but generates some slight modification in the iron electronic structure in this configuration. The EELS spectra essentially reflect the increasing degree of valence-electron delocalization and the diminishing number of oscillating electrons in going from Fe-Si(6 at. %) to $FeSi_2$. The results are discussed in comparison with other transition-metal silicides and with related iron compounds as well as on the basis of crystallographic data.

I. INTRODUCTION

A combination of surface spectroscopy techniques has been applied to investigate the main aspects of the chemical bond at interfaces. A special application is segregation studies of interstitial and substitutional "*sp*" impurities on free surfaces of α-iron in order to elucidate the elemental composition of the surface region and the bonding state of the segregated species. The interest in this topic is on one hand due to the strong correlation between grain-boundary segregation[1] and such phenomena as temper embrittlement[2–8] and creep embrittlement.[9–11] On the other hand, segregated nonmetallic impurities on free-transition-metal surfaces can play an important role in phenomena such as chemisorption,[12–14] corrosion,[15–17] adhesion,[18] and catalytic processes.[19–21]

For the segregation system Fe-P (Ref. 22) we have recently published an electron spectroscopic study wherein we demonstrated the usefulness of comparing samples with metalloids dissolved in the bulk to bulk compounds formed by the same elements. This concept can also be applied to silicon segregation onto α-iron surfaces. Owing to technological importance in device applications, the structural and electronic properties of numerous metal silicides[23–27] and metal-silicon interfaces[28] have been successfully characterized by surface-sensitive methods and modeled by theoretical calculations. In addition, the lack of extended experimental and theoretical studies concerning the iron-silicide surfaces, apart from Fe_3Si,[29–32] has stimulated us to investigate in more detail the binding of silicon and iron atoms on the surfaces of different iron silicides.

II. EXPERIMENTAL

The x-ray photoelectron spectroscopy (XPS), Auger-electron spectroscopy (AES), and electron-energy-loss spectroscopy (EELS) experiments were performed in a Leybold-Heraeus LHS 10 system consisting of a stainless-steel vacuum chamber with a 180° hemispherical analyzer and a valveless load-lock system including preparation chamber. The system is capable of a base pressure below 1×10^{-8} Pa in the analyzer chamber (ion-getter pumped) and 1×10^{-7} Pa in the preparation chamber (turbomolecular pumped). The specimens of about 10×10 mm^2 size are mounted on a direct heating sample rod, permitting a maximum sample temperature of 800 °C. The electron spectra were excited in glancing incidence and recorded in normal emission with an analyzer pass energy of 50 eV except for the Auger spectra which were recorded at constant $\Delta E/E$. Further details of the experimental setup have been described previously.[22] Energy calibration was based on the following photoline positions for copper metal: Cu $2p_{3/2}=932.6\pm0.1$ eV, Cu $3s=122.6\pm0.1$ eV, and Cu $3p_{1/2,3/2}=77.2\pm0.05$ and 75.1 ± 0.05 eV. The Fermi level was determined by frequent analysis of the valence-band spectra of clean nickel or iron material. The nonmonochromatized Mg $K\alpha$ radiation (1253.6 eV) gives a 1.1-eV full width at half maximum (FWHM) for Au $4f_{7/2}$ in the analyzer mode with a 50-eV pass energy. A deconvolution procedure assuming a Gaussian line profile of 0.7-eV FWHM for the instrumental resolution and intrinsic linewidth results in a 0.8-eV FWHM for Au $4f_{7/2}$. Supplemental angle-integrated UPS experiments were carried out in a Vacuum Generators ESCALAB 5 equipped

with a uv discharge lamp.

The samples under investigation, Fe-Si(6 at. %), Fe_3Si, FeSi, and $FeSi_2$, were produced by melting high-purity iron and silicon material and applying the Bridgeman method for producing monocrystals. This procedure was successful with the exception of the $FeSi_2$ specimens which consisted of polycrystalline material. The single crystals were cut by spark erosion to within $\pm 0.5°$ of the (100) surface orientation. The silicon enrichment of the Fe(100) surface was achieved by heating a silicon-doped iron single crystal ($c_{Si}=6$ at. %, i.e., within the solubility range of silicon in α-iron) to 600 °C. At equilibrium saturation, a $c(2\times 2)$ superstructure of Si on Fe(100) was detected by low-energy electron-diffraction (LEED) experiments. This result implies that the silicon enrichment at saturation corresponds to a surface coverage of half a monolayer. The mechanically polished surfaces of the specimens were prepared *in situ* by short soft-argon or -neon sputtering at elevated temperatures. Surface cleanliness was checked for all the samples under investigation by AES (Fig. 1). The elemental surface composition was analyzed by ion scattering spectroscopy (ISS) experiments and correlated to AES peak-height ratios in order to make sure that during sputtering no depletion of iron or silicon took place.

III. RESULTS

A. Photoelectron spectra

All silicon and iron core levels, Auger transitions, and valence-band distributions available to Mg $K\alpha$ radiation were analyzed for the silicides, pure iron, pure silicon, and the iron-silicon segregation system. Wide-scan x-ray photoemission spectra of the iron surface saturated with silicon at equilibrium and of the silicides are shown in Fig. 2.

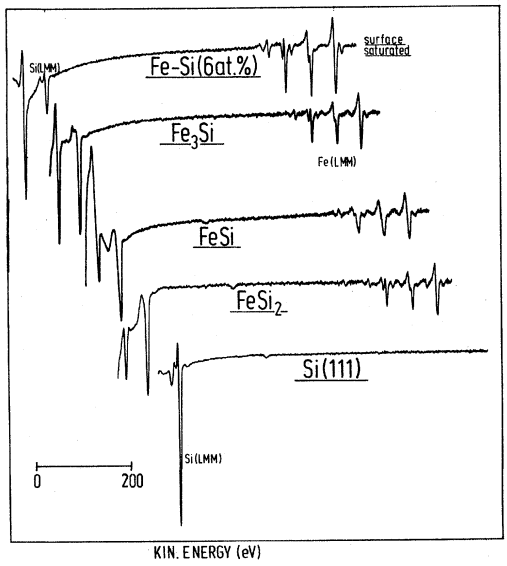

FIG. 1. Electron-excited Auger spectra of the Fe(100)-Si[$c(2\times 2)$], Fe_3Si(100), FeSi(100), $FeSi_2$(poly), and Si(111) surfaces. $E_p=2.5$ keV and $U_{mod}=2V_{pp}$.

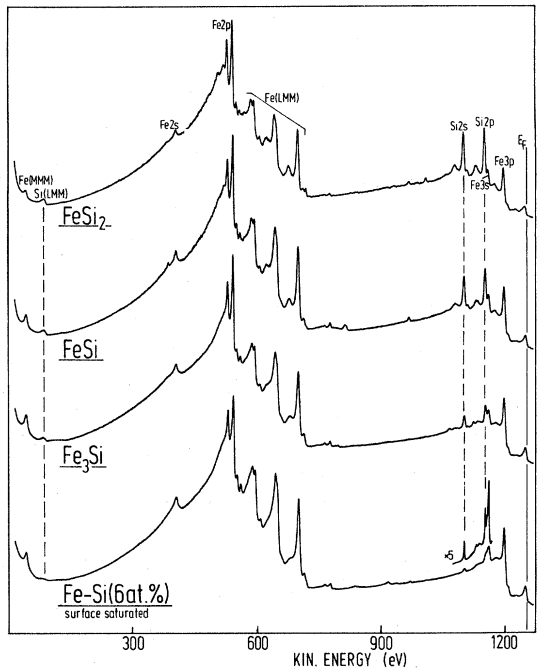

FIG. 2. Wide-scan x-ray photoemission spectra [Mg $K\alpha$, $EN(E)$ mode] of the Fe(100) surface saturated with segregated Si ($c_{Si}=6$ at. %) and of the iron silicide surfaces.

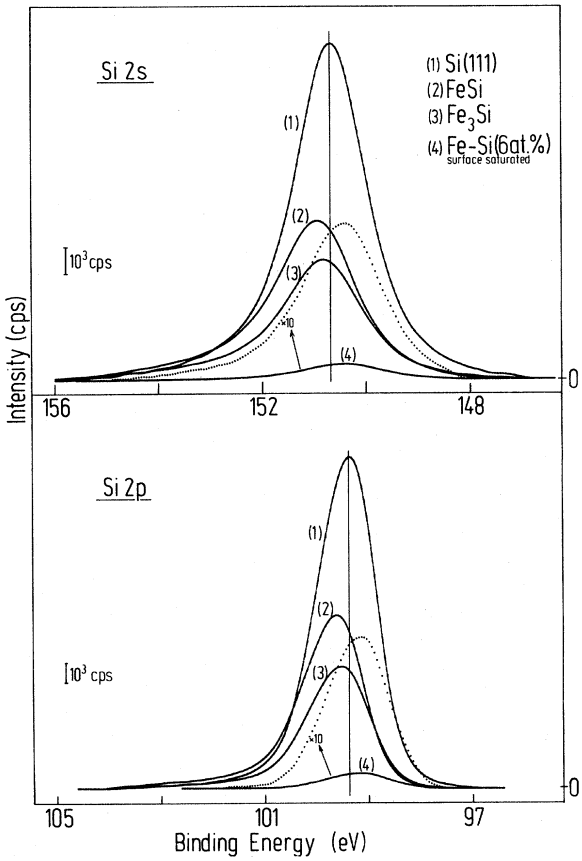

FIG. 3. Si 2*s* and Si 2*p* core-level spectra (Mg $K\alpha$—excited) of Si segregated onto the Fe(100) surface ($\cdots$ enlarged by 10 times) and of Fe_3Si, FeSi, and pure Si surfaces—after background subtraction. Peak heights represent the absolute photoemission intensities.

For information concerning the bonding states of iron and silicon, the energy positions and the line shapes of selected core levels and the valence band are taken into account. In Fig. 3 the Si 2*s* and Si 2*p* core levels of Si in the segregated state, in the silicides, and in pure silicon are shown. As compared to pure silicon, the Si 2*s* and Si 2*p* core levels in the silicides are shifted to higher binding energies, whereas the photoemission line of the segregated species has a lowered binding energy. The Si core levels of $FeSi_2$ (not shown) are within accuracy identical in binding energy to those of FeSi. Corresponding energy shifts are also detected for the iron lines. The binding-energy values for the iron and silicon core levels Fe $2p_{3/2}$, Fe 3*p*, Si 2*s*, and Si 2*p* are summarized in Fig. 4 as a function of the Si bulk concentration. The variations of the linewidths are shown in Fig. 5. The FWHM's of the silicon core levels are smallest for pure silicon and increase with higher Si bulk concentration in the samples: for Si 2*s* from 1.7 (pure Si) to 1.9 eV ($FeSi_2$), and for Si 2*p* from 1.35 to 1.45 eV. The FWHM changes for Fe 3*p* are similar, except for the $FeSi_2$ specimen: From 2.55 eV in pure iron there is an increase up to 2.7 eV in FeSi, and a slight drop to 2.65 eV for $FeSi_2$. The variations of the Fe $2p_{3/2}$ linewidths are more drastic: The Fe $2p_{3/2}$ FWHM decreases from 2.15 eV in pure iron to 1.6 eV in $FeSi_2$.

The x-ray photoemission valence-band spectra of Fe, surface-saturated Fe-Si(6 at. %), Fe_3Si, FeSi, and $FeSi_2$ are compared in Fig. 6. The valence bands of the silicides and the silicon-saturated Fe(100) surface retain the high electron densities at the Fermi energy E_F as in pure Fe, but some intensity modifications occur in the binding-energy region between $\simeq$1 and $\simeq$4 eV below E_F. The 3*d* valence-band peak is at the same energy position as that of iron, viz., $\simeq$0.7 eV. By subtracting the valence-band spectrum of clean iron from the silicide and silicon-saturated Fe(100) valence-band spectra, the additional features due to silicon-induced states and/or due to changes in the iron density of states (DOS) become more pronounced (Fig. 7). The features between 9.1 and 9.6 eV in the silicide spectra originate from electron emission out of the Si 3*s* level. The nature of the structures at lower binding energies is more complex. At first sight, the peak at about 2 eV binding energy can be attributed to a modified Fe 3*d* DOS, whereas the lines with energies between 3.3 and 4.4 eV are composed of silicon and iron states. The magnitude of the Si 3*p* contribution to the feature at about 3.5 eV below E_F is difficult to estimate for the Fe-Si(6 at. %) and the Fe_3Si specimens, because of the very low photoionization cross section at this high photon excitation energy (Cooper minimum). With increasing silicon con-

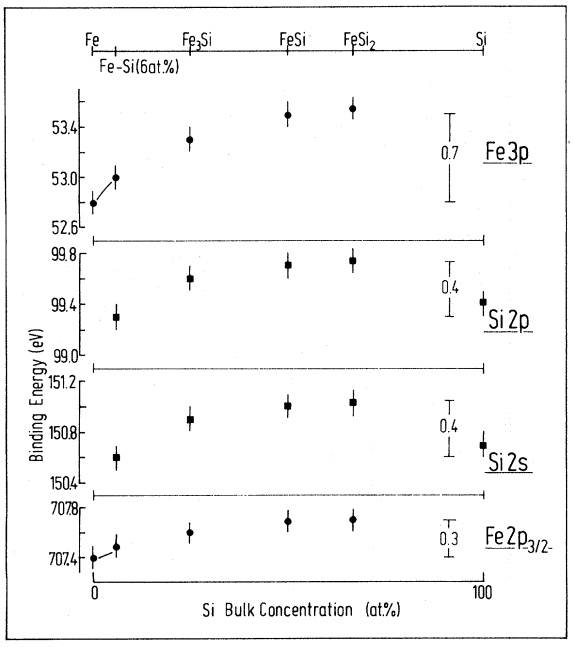

FIG. 4. Binding energies of the Mg $K\alpha$—excited Fe 3*p*, Si 2*s*, Si 2*p*, and Fe $2p_{3/2}$ core levels as a function of silicon bulk concentration for pure Fe, the Fe surface saturated with segregated Si, Fe_3Si, FeSi, $FeSi_2$, and pure Si.

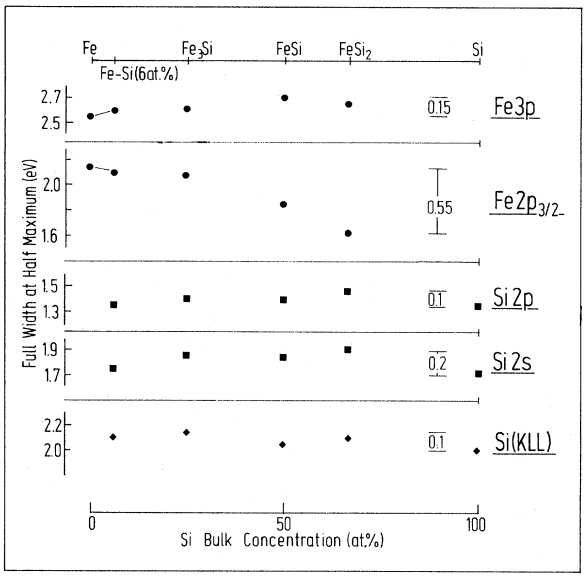

FIG. 5. FWHM of the iron and silicon core levels and of the Si(*KLL*) transition as a function of Si bulk concentration in iron.

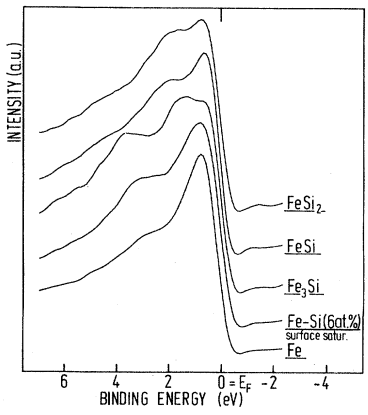

FIG. 6. X-ray photoemission valence-band spectra of $FeSi_2$, FeSi(100), Fe_3Si(100), Fe(100)-Si[$c(2\times2)$], and clean Fe. Spectra are deconvoluted.

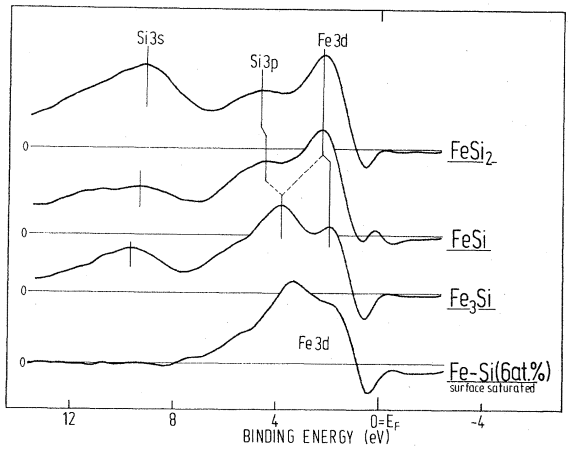

FIG. 7. Valence-band difference spectra: The valence band of clean iron has been subtracted from those of iron silicides and Fe(100)-Si[$c(2\times2)$].

tent ($FeSi$, $FeSi_2$), the Si $3p$ state seems to become more dominant accompanied by a shift to higher binding energies.

The location of the Si $3p$ photoemission line in this binding-energy region can be demonstrated by performing He I photoemission spectroscopy. In Fig. 8, He I and Mg $K\alpha$ valence-band spectra of the Fe(100)-Si[$c(2\times2)$] surface are compared. In the angle-integrated ultraviolet-photoemission spectrum, two silicon-induced photoemission states are detected: Si $3p$ and Si $3s$ situated at 4.0 and 9.2 eV below E_F, respectively. Recently performed photoemission experiments on this Fe(100)-Si[$c(2\times2)$] surface using sychrotron radiation with photon energies $12 \leq \hbar\omega \leq 120$ eV show the outer-shell Si photoemission lines to be located at the same binding-energy positions in the valence-band spectra for $\hbar\omega \leq 28$ eV. The Si peak intensities nearly vanish for photon energies greater than or equal to 30 eV due to the very low photoionization cross sections. Therefore the Mg $K\alpha$—excited valence-band spectrum (Fig. 8) reflects essentially the modified iron

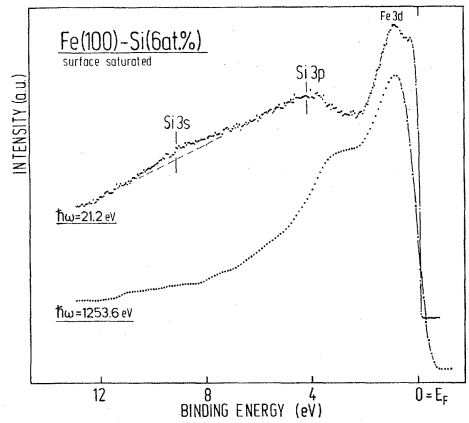

FIG. 8. He I and Mg $K\alpha$—excited valence-band spectra of the Fe(100)-Si[$c(2\times2)$] surface.

DOS caused by the interaction of Si surface atoms with iron atoms on the (100) surface. In the case of Fe_3Si (Fig. 7), the shape of the Si $3p$ photoemission line is still suppressed by the iron $3d/4s$ states, while the separation between Si $3p$ and the Fe valence levels becomes more distinct in FeSi and $FeSi_2$.

B. Auger spectra

AES of silicon core-valence and core-core transitions are investigated with regard to obtaining supplemental information about Si valence states and Si core levels. Because of the better signal-to-noise ratio, the Si($L_{23}VV$) spectra were excited by electron bombardment ($1.5 \leq E_p \leq 2.5$ keV), whereas the Si(KLL) lines were generated by bremsstrahlung of the Al anode. The $L_{23}VV$ Auger line shapes of silicon on iron-silicide surfaces, in pure silicon and on the Si-saturated Fe(100) surface, are compared in Fig. 9. The low-energy features in the Si(LVV) spectrum turned out to be complex, e.g., by reason of the Fe(M_1VV) overlap. Characteristic fine structures on the high-kinetic-energy side of the Si($L_{23}M_{23}M_{23}$) Auger line are most readily detectable in the second-derivative mode (Fig. 10). As can be seen in Fig. 10 the Auger spectrum of the Fe_3Si(100) specimen exhibits a resolved feature 4.3 eV above the main transition—labeled A in Fig. 10. For FeSi a corresponding structure is still discernible and reproducible. This is indicated in Fig. 10 by the dashed lines marking the alteration in slope. The silicon in the segregated state on the Fe(100) surface is characterized by a broadened tail on the high-kinetic-energy side of the main transition compared to pure silicon.

With increasing silicon content in the specimens, the main Si Auger transition $L_{23}M_{23}M_{23}$ shifts to higher ki-

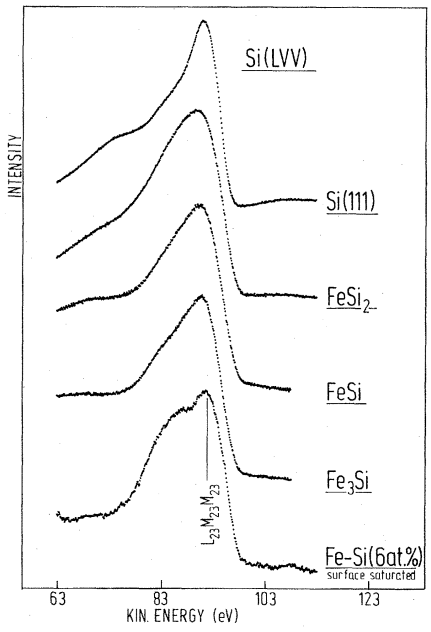

FIG. 9. Si(LVV) Auger spectra of clean Si, the iron silicides, and the Fe(100) surface saturated with segregated Si in the integral mode.

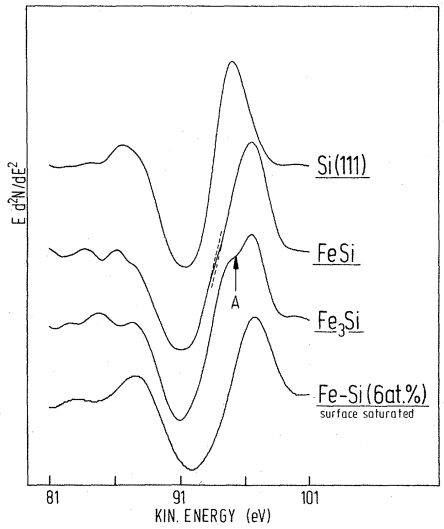

FIG. 10. Si(LVV) Auger spectra of clean Si, FeSi, Fe_3Si, and the Fe(100) surface saturated with segregated Si in the second-derivative mode. A indicates an interatomic transition (see discussion).

netic energies by 1.6 eV (Fig. 11). The values of kinetic energy are determined from the $EN(E)$ spectra. Neglecting relaxation and interaction effects in the Si($L_{23}M_{23}M_{23}$) Auger process, the binding energy of the Si 3p valence-band state can be estimated,

$$E_{\mathrm{Si}\ 3p}=0.5(E_{\mathrm{Si}\ 2p}-E_{\mathrm{Si}(L_{23}M_{23}M_{23})})\ , \tag{1}$$

where $E_{\mathrm{Si}\ 2p}$ means the core-level binding energy as measured by XPS (see Sec. III A). From Eq. (1) we obtain the following binding energies for the Si 3p state: 3.8 eV (Fe(100)-Si[$c(2\times2)$]), 4.4 eV (Fe_3Si), 4.6 eV (FeSi), 4.8 eV ($FeSi_2$), and 4.0 eV [Si(111)]. They are in good agreement with our UPS and XPS data (see Figs. 7 and 8).

The dependence of the Si($KL_{23}L_{23}$) kinetic energies on the Si bulk concentration is shown in the lower part of Fig. 11. From this and the experimental Si 2p binding energies the modified Auger parameter α^* (Ref. 33) turns out to be 1716.9 eV (Fe(100)-Si[$c(2\times2)$]), 1716.8 eV (Fe_3Si), 1717.3 eV (FeSi), 1717.1 eV ($FeSi_2$), and 1716.2 eV [Si(111)]. The value for pure silicon is in excellent agreement with the one calculated by Wagner and Taylor,[34] whereas no corresponding data exist in literature for iron silicides [for comparison, $PdSi_{0.6}$ — $\alpha^*=1717.3$ eV (Ref. 34)]. Assuming an overall constant binding energy of the Si 1s level [1838.9 eV (Ref. 35)], we obtain the following Auger parameter α defined by Lang and Williams[36]—expressing interaction and relaxation energies of the two-hole final state: 22.5 eV (Fe(100)-Si[$c(2\times2)$],Fe_3Si), 21.9 eV (FeSi), 22.0 eV ($FeSi_2$), and 23.3 eV [Si(111)]. The overall Si(KLL) Auger spectra are compared in Fig. 12. The escape depth of these electrons is about 30 Å. In contrast to the extremely surface-sensitive Si(LVV) transitions (escape depth $\simeq$5 Å), the KLL spectra are mainly generated by silicon species located in the subsurface region. The intensity of the volume-plasmon peak—most pronounced in the Si(111) spectrum—decreases with lower silicon content in the bulk, whereas the loss energy $\hbar\omega_p$ shifts to higher energies (Table I). The Si($KL_{23}L_{23}$) splitting due to final-state effects varies in intensity too. The intensity ratio $I_{KL_{23}L_{23}(^1D)}/I_{KL_{23}L_{23}(^1S)}$ is lower for Fe_3Si compared to that of monosilicide and disilicide, whose overall spectra are very similar.

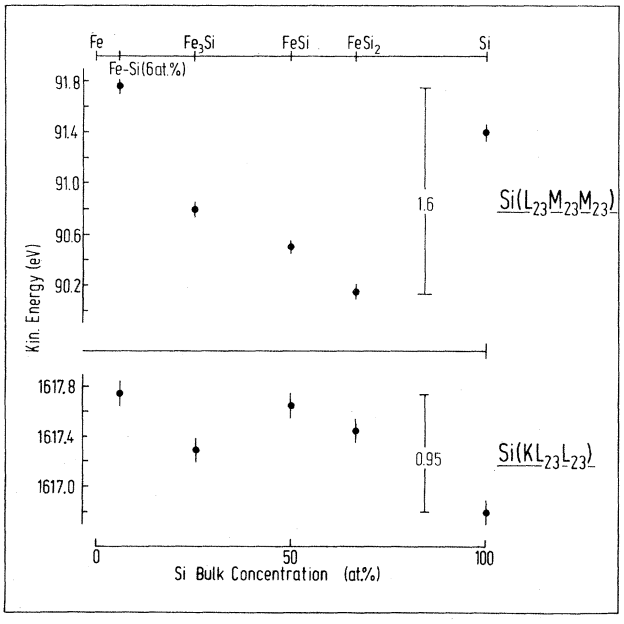

FIG. 11. Kinetic energies of the Si($L_{23}M_{23}M_{23}$) and Si($KL_{23}L_{23}$)^1D Auger transitions as a function of Si concentration in the iron bulk.

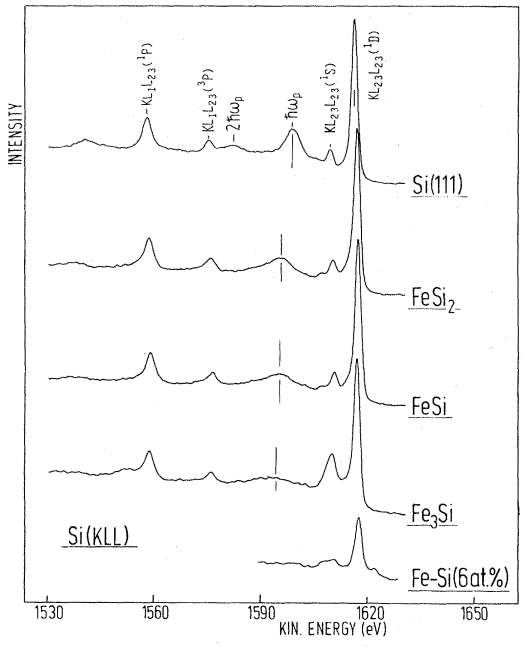

FIG. 12. X-ray-excited Si(KLL) spectra of pure Si, the iron silicides, and the Fe(100)-Si[$c(2\times2)$] specimen. Plasmon loss $\hbar\omega_p$ of the $KL_{23}L_{23}(^1D)$ Auger line is indicated.

TABLE I. Energy-loss features of Si(KLL) Auger transitions and of Si core-level spectra (eV±0.2eV). Values in parentheses are the relative intensities of the loss peaks compared to the parent peaks.

	Si($KL_{23}L_{23}$)	Si 2s	Si 2p
Fe_3Si	22.0 (11%)	22.0 (14%)	a
FeSi	21.9 (15%)	22.0 (20%)	a
$FeSi_2$	21.3 (20%)	21.2 (27%)	a
Si	17.4 (32%)	17.3 (41%)	17.4 (41%)

[a]Not unambiguously resolvable due to the strong overlap with the Fe 3s core-level spectrum.

C. Energy-loss spectra

Further insight into the electronic properties can be achieved studying electronic transitions and collective excitation modes by means of EELS. Figure 13 shows energy-loss spectra of the clean Fe(100) surface, the Fe(100)-Si[$c(2\times2)$] surface, the iron silicides, and Si(111). The characteristic energy-loss spectrum of pure silicon is mainly composed of features due to plasmon excitations. The identified plasmon loss energies (volume plasmon: $\hbar\omega_p = 17.4$ eV, surface plasmon: $\hbar\omega_s = 11.0$ eV) coincide in energy position with those found in literature.[37] The energy-loss spectra of disilicide and monosilicide resemble the pure-Si spectrum in overall shape; however, the plasmon energy $\hbar\omega_p$ is shifted to higher values by 3.4 ($FeSi_2$) and 3.7 eV (FeSi). At lower silicon content in the iron bulk, structures due to interband transitions become more dominant—with loss energies less than or equal to 20 eV. The energy-loss spectrum of a clean Fe(100) surface presented here for comparison has been interpreted in detail elsewhere.[38]

In the first-derivative mode (Fig. 14) peaks caused by one-electron transitions from silicon-induced valence states to unoccupied levels above E_F can be resolved. The silicon enrichment on the Fe(100) surface leads to two additional structures in the energy-loss spectrum labeled 1 and 2 in Fig. 14. These features at loss energies of 4.1 and 9.5 eV can be interpreted as resulting from interband transitions from the silicon resonance levels Si 3p and Si 3s into empty states above E_F. Appropriate transitions involving the Si 3s states are analyzed for the iron silicides, whereas the electron transition from the Si 3p level is no longer detectable because of the overlap with the increasing slope of the elastically scattered electron peak. Compared to pure iron the ionization loss Fe 3p ($=M_{23}$) undergoes alterations in line shape that may be due to changed final states near E_F.

IV. DISCUSSION

Compared to the standards of clean Fe(100) and clean Si(111), the photoemission lines in the core-level spectra Fe 3p, Si 2s, and Si 2p shift to higher binding energies in

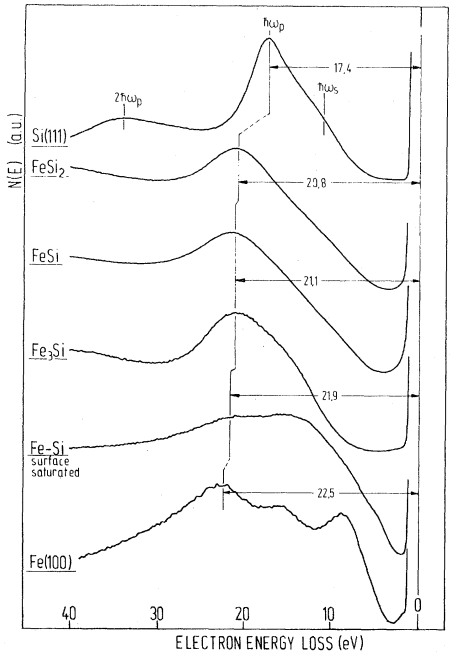

FIG. 13. Electron-energy-loss spectra of clean Si, the iron silicides, the Fe surface saturated with segregated silicon, and clean Fe [$N(E)$ mode, $E_p = 200$ eV].

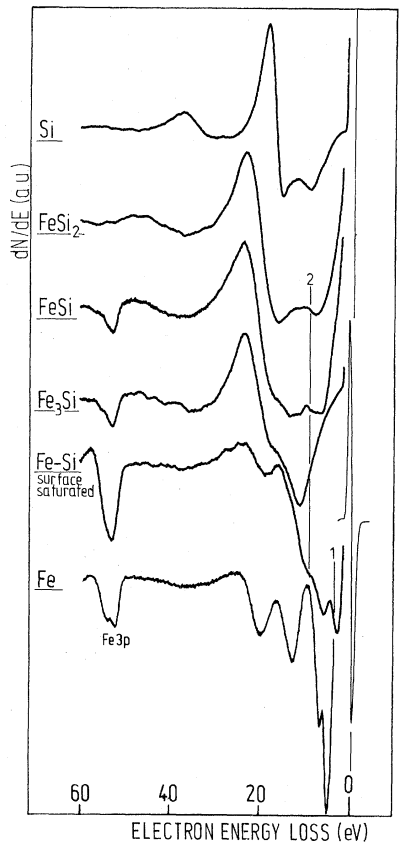

FIG. 14. Electron-energy-loss spectra in the first-derivative mode, corresponding to Fig. 13 ($E_p = 200$ eV). One-electron transitions from Si-derived valence states into unoccupied levels above E_F are labeled 1 and 2 (see text).

going from Fe_3Si to $FeSi_2$ (Fig. 4). For segregated silicon on the saturated Fe(100) surface, however, the Si 2*s* and Si 2*p* levels are somewhat lower in binding energy (approximately equal to -0.1 eV) referred to the values of pure silicon. In a zeroth-order approximation, the core-level shifts suggest a small charge transfer between iron and silicon atoms, but predominantly a homopolar bonding character.

Core-level investigations performed on Ni and Pd silicides yield similar Si 2*p* line shifts.[23,24] But some differences can be seen in comparing the Ni 3*p* behavior in Ni_2Si, NiSi, and $NiSi_2$ with the Fe 3*p* shift in iron silicides. As reported by Franciosi *et al.*,[24] a shift to higher binding energies was observed only for the nickel disilicide, whereas for lower Si concentrations the Ni 3*p* level is below the value of pure nickel. The reason for these differences between Ni and Fe silicides, in regard to dependence on Si bulk concentration, may be caused by different configuration changes due to different crystal structures.

For the Si species in the $c(2\times2)$ segregation structure on Fe(100), a laterally attractive Si-Si interaction may account for the relatively low binding energy. Recently performed angle-resolved UPS measurements show dispersion effects for the Si $c(2\times2)$ overlayer on Fe(100) of about 0.8 eV,[39] indicating silicon-silicon interaction. The 0.2-eV binding-energy shift of the Fe 3*p* core level in this state can be interpreted as being due to the slightly modified charge distribution around the Fe surface atoms influenced by the Si overlayer.

From Fig. 5 the changes in linewidths of the Si and Fe core levels, as a function of silicon bulk content, are most pronounced for the Fe $2p_{3/2}$ photoemission line. The decrease of the Fe $2p_{3/2}$ FWHM with increasing Si concentration can be interpreted by taking crystallographic data of the iron silicides into account (cf. Appendix). The linewidth of pure iron is established by solid-state effects, i.e., the metallic bonding within the iron bcc lattice. In going from Fe_3Si to $FeSi_2$, the interaction of adjacent Fe atoms becomes less because the coordination number of the Fe nearest neighbors decreases and in addition their mutual distance grows. The Fe $2p_{3/2}$ line shape of the higher silicides shows a more atomiclike character despite an increase of the spatial density of Si atoms. This suggests that the Fe-Si interaction is relatively weak, but significant localized silicon—silicon bonding occurs for FeSi and $FeSi_2$. Joyner *et al.*[40] report on comparable mechanisms for the iron-boron system in the crystalline Fe_2B and FeB phases.

From the XPS core-level data there is no indication of a second state of segregated silicon in the near-surface region, in contrast to recently performed studies of the iron-phosphorus segregation system.[22] The phosphorus occurs in two states as characterized by P 2*s* and P 2*p* core-level spectra: a chemisorbed state on top of the surface and a second state in the subsurface. For segregated silicon, a line-shape analysis of Si 2*s* and Si 2*p* photoemission lines reveals only one bonding state and did not show any remarkable changes for Si as bonded in the silicides. In order to fit the experimental Si 2*s* line shape to analytical curves, an additive composition of Gaussian and Doniach-Šunjić line (asymmetry parameter 0.15) yields a good fit as demonstrated in Fig. 15. The low-binding-energy part turned out to be a 30% Gaussian with 1.8 eV FWHM.

The experimental valence-band spectra (Figs. 6—8) yield some complementary information on the chemical bonding between iron and silicon. For Si in the segregated states on Fe(100), the ultraviolet photoemission spectrum (Fig. 8) shows two silicon-derived features and a modified Fe 3*d* valence band (emission maxima: 0.4 and 0.8 eV) compared to results of clean iron. While the Si 3*s* level is more or less isolated from the iron valence states, the Si 3*p*—induced structure at 4.0 eV below E_F is superimposed on the majority bands of Fe, indicating some hybridization effects. Because of the very low photoionization cross section of the Si 3*p* level for x-ray excitation, the x-ray photoemission valence-band spectrum (Fig. 8) reflects only Fe $3d/4s$ energy-distribution curves (EDC's) where the spin-up band becomes more intense accompanied by a shift from 2.5 eV (clean Fe) to $\simeq$3.2 eV below E_F. As illustrated in Figs. 6 and 7, the valence-band emission of Fe_3Si shows pronounced features at 0.7, 1.8, and 3.7 eV. Whereas the first two peaks in the EDC's are due to Fe 3*d* states, the structure at 3.7 eV is caused by an overlap of the Si 3*p* and the Fe $3d/4s$ emission. The separated Si 3*s* photoemission line appears 9.4 eV below E_F. From the Fe_3Si valence-band data and from the results on the core levels, we suggest that the metallic bonding character between the iron atoms of elemental iron is retained in Fe_3Si accompanied by a slight charge transfer from Fe to Si. Such bonding was theoretically demonstrated for Ni_2Si by Bisi and Calandra.[25]

The valence-band spectra of FeSi and $FeSi_2$ are characterized by a high DOS 0.7 eV below E_F and a greater

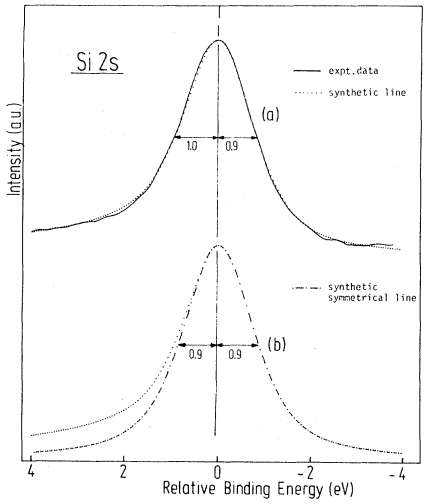

FIG. 15. Mg $K\alpha$—excited Si 2*s* core level of the Fe(100)-Si[$c(2\times2)$] specimen ($c_{Si}=6$ at. %): (a) Comparison of the experimental data (solid line) with a synthetic line (dotted line) which is additively composed of a 30% Gaussian and 70% Doniach-Šunjić line (asymmmetry parameter 0.15); (b) Symmetrical synthetic line (dashed-dotted) as received from mirroring the low-binding-energy part at the intensity maximum of the asymmetrical synthetic line.

separation of the Si $3p$ valence level from the Fe $3d/4s$ states (Fig. 6). This behavior coincides with increasing Fe-Si distances and the increasing atomic density of Si in the crystal structures of the silicides (cf. Appendix). In FeSi and especially in $FeSi_2$ the silicon-silicon interaction becomes considerably greater and causes covalent Si—Si bonding, very similar to the bonding of boron in the iron borides.[40] The mutual silicon interaction results in changes in the electron configuration of the Fe atoms.

Band-structure calculations for the higher iron silicides are not available to our knowledge, but for the intermetallic compound MnSi, which crystallizes in the same B-20 structure type as FeSi, a high DOS at the Fermi level was calculated by a self-consistent augmented-plane-wave (APW) method.[26] Photoemission experiments recently performed on fractured nickel silicide surfaces at lower photon energies[24] differ qualitatively from our valance-band results because of the very low DOS near E_F. The Ni $3d$ bands shift with increasing Si bulk concentration from 1.3 eV for Ni_2Si to 3.2 eV below E_F for $NiSi_2$. This different behavior of Ni and Fe silicides may be established by the different crystal structures of the corresponding silicides: for the Ni silicides we note the following: (a) The Ni nearest-neighbor (NN) distance is only slightly larger in Ni_2Si and NiSi than in Ni metal, while in $NiSi_2$ the NN distance is increased by 53% compared to Ni; (b) the Ni coordination number for Ni_2Si and NiSi decreases substantially relative to Ni metal, and in $NiSi_2$ the Ni atoms occupy an fcc metal sublattice as in fcc Ni.[24] This suggests that the Ni d character becomes more atomiclike as the Si concentration increases. For the Fe silicides, however, (a) the Fe NN distance is slightly smaller in Fe_3Si than in Fe metal, but the NN distance is largest in FeSi with an increase of 10% compared to Fe and is increased about 8% in $FeSi_2$ relative to elemental Fe; (b) the Fe coordination number in the silicide compounds attains values between 4 and 6 (and 8 for the Fe_B atoms in Fe_3Si) (cf. Appendix). Therefore the atomiclike character is not so distinct in the iron-silicon compounds, which is obviously reflected in the d-derived valence bands. On the other hand, the silicon-silicon interaction in the iron monosilicide and disilicide seems to play a more important role compared to the nickel silicides. As mentioned above, valence-band investigations of iron borides[40] and theoretical studies of MnSi (Ref. 26) are more similar to our appropriate valence-band shapes of iron silicides than are the Ni silicide valence-band spectra.

A different behavior has also been reported for iron and nickel disulfides FeS_2 and NiS_2,[41,42] both of which have the pyrite structure. From photoemission spectra excited by synchrotron radiation the Fe $3d$ level has been found 0.8 eV below E_F, whereas the Ni $3d$ levels are situated between 2.2 and 3.0 eV below E_F. According to Li *et al.*[42] for the pyrites, this difference is due to the two additional $3d$ electrons in the Ni cation (compared with Fe) which go into broad antibonding e_g levels.

Auger spectra were analyzed to provide additional information on chemical bonding in iron silicides and in the iron-silicon segregation system. The fact that the Fe(LMM) transitions appear within ± 0.2 eV of the same energies in Fe, Fe-Si(6 at. %), and the silicides sustains the conclusions from x-ray photoemission core-level and valence-band spectra. Similar behavior of the Fe(LMM) transition is observed for iron borides.[40] The kinetic-energy position of intra-atomic core-valence transitions Si($L_{23}M_{23}M_{23}$) directly reflects the shifts in Si $2p$ and Si $3p$ binding energies for the different silicides and the segregated silicon on Fe(100).

The characteristic alterations in the Si(LMM) line shape are assumed to be due to changes in Si valence orbital composition caused by metal-Si interaction.[43] The weak features at the high-energy side of the main Si($L_{23}M_{23}M_{23}$) Auger transition, which are only clearly visible for Fe_3Si in the second-derivative spectrum (Fig. 10), can be discussed alternatively. For comparison in the case of Pd_3Si (Ref. 24) and Pd_2Si (Ref. 44) a corresponding structure is observed about 4—5 eV above the central Si(LMM) peak. Based on partial-state-density calculations,[45] for the Pd-Si compounds the Si $3p$ states form two well-defined groups straddling the d band with locations near E_F ($E_B=0$ eV) and at 5 eV below E_F, i.e., bonding and antibonding states are formed by hybridization of the Si $3p$ and Pd $4d$ electrons. Conclusively for Pd_2Si the feature at the high-energy side of the main Si(LMM) Auger peak is due to transitions involving two occupied antibonding Si $3p$ states. For Fe_3Si, however, electronic energy-band calculations have shown that states corresponding to the antibonding combination of the Si $3p$ and Fe $3d$ orbitals are located above E_F.[32] Therefore Auger processes in which the antibonding Si $3p$ level is involved are assumed to be negligible for the iron silicides.

Alternatively an interpretation referring to a model proposed by Salmerón *et al.*[46] seems to be more appropriate for the iron-silicon system. In this model features at the high-energy side of the main $L_{23}M_{23}M_{23}$ peak are caused by interatomic transitions involving the iron $3d$ electrons in the Auger process. This interpretation was successfully applied by the authors to the iron-phosphorus segregation system.[22] In the case of silicon in iron the structures on the high-energy side of the main Si($L_{23}M_{23}M_{23}$) Auger transition are very weak, indicating only a small interatomic transition probability. Taking into account the crystal structure and valence-band data of the silicides, the interatomic Auger process should be strongest for Fe_3Si because of the high spatial iron density around the isolated Si atoms, and the iron valence states are most strongly modified compared to pure iron. Assuming the structure (A) at 96.3 eV in Fig. 10 to be caused by a transition involving double participation of the Fe $3d$ state results in a calculated iron $3d$ level located 1.6 eV below E_F. This coincides excellently with a strong x-ray photoemission valence-band feature detected at 1.7 eV below E_F for Fe_3Si (Fig. 6).

Owing to the growing silicon-silicon interaction with increasing silicon content between Fe_3Si and $FeSi_2$, the interatomic transitions involving the Fe $3d$ level become smaller in intensity, thus expressing the diminishing interaction of iron and silicon atoms. Consequently the Si(LVV) spectrum of pure silicon should not show any appropriate fine structure. This is clearly verified in Fig. 10. From the line shape of segregated silicon on Fe(100) at saturation—which mostly resembles that of pure

TABLE II. Crystallographic data and electrical resistivity of iron and the iron silicides. For FeSi and $FeSi_2$ the lattice dimensions depend on the Si content in the bulk within a small range of stoichiometric composition: iron-rich (higher value) or silicon-rich (smaller value). Electrical resistivity is given for room temperature.

	Structure type[a]	Space group[b]	Lattice dimensions (Å)[c]	Electrical resistivity (10^{-6} Ω cm)[a]
α-Fe	bcc	Im3m	$a=2.8662$[b]	9.8[d]
Fe_3Si	DO_3[e]	Fm3m	$a=2.8277$	55
FeSi	B-20	$P2_13$	$a=4.488-4.483$	240
$FeSi_2$	tetragonal	P4/mmm	$a=2.698-2.683$ $c=5.141-5.127$	350

[a]Reference 50, unless stated otherwise.
[b]P. Eckerlin and H. Kandler, in *Landolt-Börnstein, Group III, edited by K.-H. Hellwege and* A. M. Hellwege (Springer, Berlin, 1971), Vol. 6, p. 581.
[c]Reference 49, unless stated otherwise.
[d]C. Kittel, *Introduction to Solid State Physics* (Wiley, New York, 1976).
[e]Reference 29.

silicon—we propose that for segregated silicon the laterally attractive silicon-silicon interaction plays a significant role compared to the bonding strength of silicon to iron surface atoms. This is suggested by our photoemission data too.

In going from Fe_3Si to Si(111), the corresponding Si(*KLL*) Auger spectra exhibit electron-energy-loss features which increase in intensity and simultaneously shift to lower loss energies (Fig. 12 and Table I). In comparison to the well-known Auger spectrum of pure silicon,[47] the loss structures in the spectra of the iron silicides are mainly due to bulk-plasmon excitations. Plasmon peaks with similar loss energies are also detected in the Si 2*s* and Si 2*p* core-level spectra (Table I) and in the electron-stimulated energy-loss spectra (Fig. 13). As the silicon content is increased between Fe-Si(6 at. %) and $FeSi_2$, the characteristic loss features in the energy-loss spectra are mainly caused by collective excitations—those dominating over one-electron transitions. Since the plasmon energy is directly related to the number of oscillating electrons,[48] the decreasing loss energy $\hbar\omega_p$ as a function of the silicon concentration in the bulk indicates that the quantity of itinerant electrons decreases. At the same time the degree of electron delocalization is enhanced in going to the higher silicides because the intensity of the $\hbar\omega_p$ peak increases relative to the intensity of the one-electron transitions. The effect of increasing plasmon intensity in going from Fe_3Si to $FeSi_2$ is more obvious in the Si(*KLL*) and the Si 2*s* spectrum (see Table I). In the first-derivative mode of the energy-loss spectra, one-electron transitions can be analyzed in addition to the plasmon peaks (Fig. 14). The iron-induced structures in the energy-loss spectra of the clean iron surface have been discussed in detail elsewhere.[38] Extra features due to electronic transitions from occupied Si valence-band states to unfilled levels above E_F are marked by 1 and 2 in Fig. 14. In the case of surface-enriched silicon on Fe(100)-Si[$c(2\times2)$], the 4.1- and 9.5-eV loss peaks originate from

TABLE III. Atomic distances *d* in iron and the iron silicides. Number of neighboring atoms is given in parentheses. Unless stated otherwise the values have been computed from the data given in Ref. 49.

	Environment of Fe atoms		Environment of Si atoms	
	$d_{Fe\text{-}Fe}$ (Å)	$d_{Fe\text{-}Si}$ (Å)	$d_{Si\text{-}Si}$ (Å)	$d_{Si\text{-}Fe}$ (Å)
α-Fe	2.49 (8) 2.87 (6)			
Fe_3Si:Fe_A	2.45 (4)	2.45 (4) 2.83 (6)	4.00 (12)	2.45 (8)
Fe_3Si:Fe_B	2.45 (8)	2.83 (6)	4.00 (12)	2.83 (6)
FeSi[a]	2.75 (6)	2.29 (1) 2.34 (3) 2.52 (3)	2.78 (6)	2.29 (1) 2.34 (3) 2.52 (3)
$FeSi_2$	2.68 (4) 3.79 (4) 5.13 (2)	2.35 (8) 4.20 (8)	2.36 (1) 2.68 (4) 2.77 (1)	2.35 (4) 4.20 (4) 4.46 (8)

[a]Reference 51.

electron transitions from Si $3p$ (4.0 eV below E_F) and Si $3s$ (9.2 eV below E_F) to Fe $3d$ (just above E_F). These interband transitions become weak in the energy-loss spectra of the silicides because the collective character is now more predominant.

V. CONCLUSIONS

Slight shifts of the silicon and iron core levels to higher binding energies in going from Fe_3Si to $FeSi_2$ indicate a small charge transfer from iron to silicon atoms. The high DOS of the nonbonding $3d$ level 0.7 eV below E_F is consistent with the intermetallic properties of the iron silicides. In contrast to Fe_3Si where the iron—silicon bonding is predominant, the silicon-silicon interaction is prevailing in the monosilicide and disilicide. The interatomic transitions in the Si(LMM) Auger spectra involving bonding Fe $3d$ valence states ($\simeq$1.7 eV below E_F) sustain this result.

In the case of segregated silicon on Fe(100) at surface saturation the x-ray photoemission valence-band spectra reveal changes in the d-electron band's substructure. Photoemission experiments at photon energies less than or equal to 30 eV show the Si $3p$ and Si $3s$ level at 4.0 and 9.2 eV below E_F, respectively. Because of dispersion effects (approximately equal to 0.8 eV) for the silicon p-derived bands in angle-resolved UPS experiments[39] and the lower binding energy of the Si core levels with regard to pure silicon, we propose a relatively strong lateral interaction of the segregated Si surface atoms, compared to the bonding strength between silicon and iron atoms at the surface. The bonding is prevailingly homopolar.

From the discrete energy-loss features in the Si(KLL), the Si core level, and the energy-loss spectra, it was concluded that the itinerant character of the valence electrons increases when going from Fe-Si(6 at. %) to $FeSi_2$, whereas simultaneously the number of oscillating electrons decreases. Overall analysis of the energy-loss spectra indicates a more free-electron-like behavior for the electronic properties of the monosilicide and disilicide.

ACKNOWLEDGMENTS

This study was initiated by H. J. Grabke. We are grateful to H. Viefhaus and to H. Kudielka for helpful discussions. This work was supported by the Deutsche Forschungsgemeinschaft.

APPENDIX: SOME PROPERTIES OF THE IRON SILICIDES

The bulk crystal structures of Fe_3Si, FeSi, and $FeSi_2$ are shown in Fig. 16. Tables II and III give some additional data. The DO_3-type lattice of Fe_3Si evolves from the Fe bcc structure by the continual substitution of Fe and Si atoms, alternately, for the body-centered sites, which is accompanied by a shrinkage of the unit cell.[49] Nearly one-third of the iron atoms in α-iron can be replaced by silicon. For Si concentrations of 25 at. %, the structure is completely ordered as shown in Fig. 16, whereas for lower and higher Si content the structure becomes disordered. There exist two different metal-atom sites in Fe_3Si, labeled Fe_A and Fe_B in Fig. 16. The Si atoms are completely isolated and are only surrounded by Fe atoms. Other representatives of the DO_3-type lattice are Fe_3Al and Mn_3Si.[29]

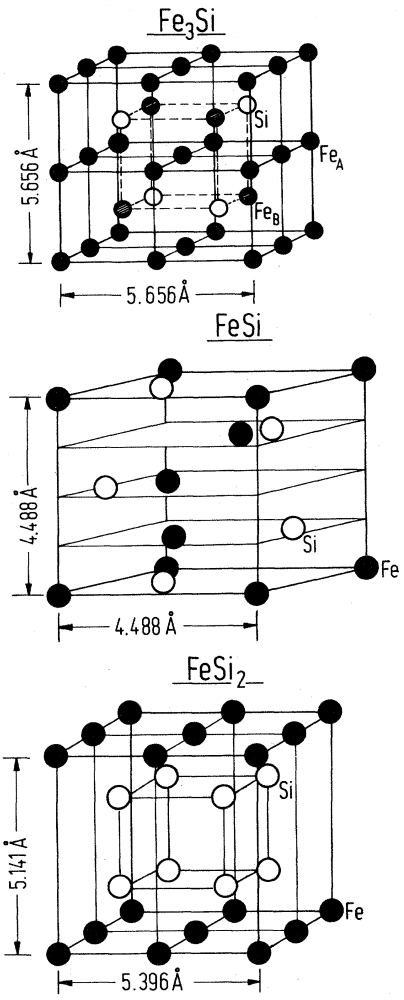

FIG. 16. Bulk crystal structures of the iron silicides. Full circles: iron atoms. Open circles: silicon atoms. (In Fe_3Si, Fe_A and Fe_B are two different iron-atom sites.)

In FeSi the Si atoms are still isolated and bonded to metal atoms only.[50] The arrangement of atoms has been studied in detail by Pauling and Soldate.[51] FeSi is a narrow-gap semiconductor (gap width of 0.05 eV).[26] Other representatives of the B-20 structure of FeSi are CoSi and MnSi. Within the $FeSi_2$ lattice there is a structure of uniplanar iron-iron layers with Si forming adjacent pairs, i.e., the bonding of Si atoms is characterized by short Si-Si contacts.[49,50]

[1]M. P. Seah, J. Phys. F 10, 1043 (1980).
[2]I. Olefjord, Int. Metall. Rev. 4, 149 (1978).
[3]A. Joshi, in *Fractography in Failure Analysis*, edited by B. M. Strauss and W. H. Cullen (American Society for Testing and Materials, Philadelphia, 1978).
[4]R. A. Mulford, C. J. McMahon, Jr., D. P. Pope, and H. C. Feng, Metall. Trans. A 7, 1183 (1976).
[5]H. Erhart and H. J. Grabke, Metal Sci. 15, 401 (1981).
[6]H. Erhart, H. J. Grabke, and R. Möller, Arch. Eisenhüttenwes. 52, 451 (1981).

[7]J. Kameda and C. J. McMahon, Jr., Metall. Trans. A 12, 31 (1981).
[8]T. Shinoda and T. Nakamura, Acta Metall. 29, 1631 (1981).
[9]D. P. Pope and D. S. Wilkinson, in *Creep and Fracture of Engineering Materials and Structures,* edited by B. Wilshire and D. R. J. Owen (Pineridge, Swansea, 1981).
[10]M. P. Seah, Philos. Trans. R. Soc. London Ser. A 295, 265 (1980).
[11]W. Hartweck and H. J. Grabke, Scr. Metall. 15, 653 (1981).
[12]J. Benziger and R. J. Madix, Surf. Sci. 94, 119 (1980).
[13]D. W. Goodman and M. Kiskinova, Surf. Sci. 105, L265 (1981).
[14]G. A. Sargent, J. Lih-Ren Chao, and G. B. Freeman, Appl. Surf. Sci. 7, 104 (1981).
[15]J. Küpper, H. Erhart, and H. J. Grabke, Corros. Sci. 21, 227 (1981).
[16]K. L. Moloznik, G. L. Briant, and C. J. McMahon, Jr., Corros. 35, 331 (1979).
[17]E. D. Hondros and C. Lea, Nature 289, 663 (1981).
[18]W. Hartweck and H. J. Grabke, Surf. Sci. 89, 174 (1979).
[19]G. C. Bond, *Catalysis by Metals* (Academic, New York, 1962).
[20]J. C. Bayer, K. C. Stein, L. J. E. Hofer, and R. B. Anderson, J. Catal. 3, 145 (1964).
[21]H. J. Grabke, E. M. Petersen, and S. R. Srinivasan, Surf. Sci. 67, 501 (1977).
[22]B. Egert and G. Panzner, Surf. Sci. 118, 345 (1982).
[23]V. Atzrodt, T. Wirth, and H. Lange, Phys. Status Solidi A 62, 531 (1980).
[24]A. Franciosi, J. H. Weaver, and F. A. Schmidt, Phys. Rev. B 26, 546 (1982).
[25]O. Bisi and C. Calandra, J. Phys. C 14, 5479 (1981).
[26]O. Nakanishi, A. Yanase, and A. Hasegawa, J. Magn. Magn. Mater. 15-18, 879 (1980).
[27](a) *V silicides:* O. Bisi and L. W. Chiao, Phys. Rev. B 25, 4943 (1982); L. F. Mattheiss and W. Weber, *ibid.* 25, 2248 (1982); (b) *V, Ta, and Mo silicides:* J. H. Weaver, V. L. Moruzzi, and F. A. Schmidt, Phys. Rev. B 23, 2916 (1981); (c) *Co silicides:* G. Castro, J. E. Hulse, J. Küppers, and A. Rodriguez Gonzalez-Elipe, Surf. Sci. 117, 621 (1982); (d) Ni_3Si: D. M. Bylander, L. Kleinman, and K. Mednick, Phys. Rev. B 25, 1090 (1982); (e) Pd_4Si: S. D. Bader, L. Richter, M. B. Brodsky, W. E. Brower, and G. V. Smith, Solid State Commun. 37, 729 (1981).
[28](a) *V/Si:* J. G. Clabes, G. W. Rubloff, B. Reihl, R. J. Purtell, P. S. Ho, A. Zartner, F. J. Himpsel, and D. E. Eastman, J. Vac. Sci. Technol. 20, 684 (1982); (b) *V/Si and Pd/Si:* R. Purtell, J. G. Clabes, G. W. Rubloff, P. S. Ho, B. Reihl, and F. J. Himpsel, J. Vac. Sci. Technol. 21, 615 (1982); (c) *Cr/Si and Ni/Si:* A. Franciosi, J. H. Weaver, D. G. O'Neill, Y. Chabal, J. E. Rowe, J. M. Poate, O. Bisi, and C. Calandra, J. Vac. Sci. Technol. 21, 624 (1982); (d) *Ni/Si:* P. J. Grunthaner, F. J. Grunthaner, and J. W. Mayer, J. Vac. Sci. Technol. 17, 924 (1980); K. L. I. Kobayashi, S. Sugaki, A. Ishizaka, and Y. Shiraki, Phys. Rev. B 25, 1377 (1982); Y.-J. Chang and J. L. Erskine, *ibid.* 26, 4766 (1982); I. Abbati, L. Braicovich, B. De Michelis, U. del Pennino, and S. Valeri, Solid State Commun. 43, 199 (1982); (e) *Ni/Si, Pd/Si, and Pt/Si:* P. J. Grunthaner, F. J. Grunthaner, and A. Madhukar, J. Vac. Sci. Technol. 20, 680 (1982); 21, 637 (1982); (f) *Cu/Si, Pd/Si, Ag/Si, and Au/Si:* I. Abatti, G. Rossi, L. Calliari, L. Braicovich, I. Lindau, and W. E. Spicer, J. Vac. Sci. Technol. 21, 409 (1982); (g) *Mo/Si:* G. Rossi, I. Abbati, L. Braicovich, I. Lindau, and W. E. Spicer, J. Vac. Sci. Technol. 21, 617 (1982); (h) *Pt/Si:* G. W. Rubloff, Phys. Rev. B 25, 4307 (1982); (i) *Au/Si:* S. Danyluk and G. E. McGuire, J. Appl. Phys. 45, 5141 (1974); P. Perfetti, S. Nannarone, F. Patella, C. Quaresima, M. Capozi, A. Savoia, and G. Ottaviani, Phys. Rev. B 26, 1125 (1982); O. Bisi, C. Calandra, L. Braicovich, I. Abbati, G. Rossi, I. Lindau, and W. E. Spicer, J. Phys. C 15, 4707 (1982); C.-A. Chang, J. Vac. Sci. Technol. 21, 639 (1982); P. Perfetti, S. Nannarone, F. Patella, C. Quaresima, A. Savoia, F. Cerrina, and M. Capozi, Solid State Commun. 35, 151 (1980).
[29]A. Himsel, W. Blau, G. Merz, W. Niederlag, U. Querin, J. Weisbach, and K. Kleinstück, Phys. Status Solidi B 100, 179 (1980).
[30]W. Blau, A. Himsel, and K. Kleinstück, Phys. Status Solidi B 100, 541 (1980).
[31]I. N. Shabanova and V. A. Trapeznikov, J. Electron Spectrosc. Relat. Phenom. 6, 297 (1975).
[32]A. C. Switendick, Solid State Commun. 19, 511 (1976).
[33]Modified Auger parameter α^* equals the kinetic energy of Auger line plus the binding energy of the photoelectron line—as defined by C. D. Wagner, L. H. Gale, and R. H. Raymond, Anal. Chem. 51, 466 (1979).
[34]C. D. Wagner and J. A. Taylor, J. Electron Spectrosc. Relat. Phenom. 20, 83 (1980).
[35]J. A. Bearden and A. F. Burr, Rev. Mod. Phys. 39, 125 (1967).
[36]N. D. Lang and A. R. Williams, Phys. Rev. B 20, 1369 (1979).
[37]N. Nishijima, M. Miyamura, Y. Sakisaka, and M. Onchi, Solid State Commun. 25, 457 (1978).
[38]B. Egert and G. Panzner, J. Phys. F 11, L233 (1981).
[39]B. Egert, H. J. Grabke, Y. Sakisaka, and T. N. Rhodin (unpublished).
[40]D. A. Joyner, O. Johnson, and D. M. Hercules, J. Am. Chem. Soc. 102, 1910 (1980); Phys. Rev. B 24, 3122 (1981).
[41]A. Ohsawa, H. Yamamoto, and H. Watanabe, J. Phys. Soc. Jpn. 37, 568 (1974).
[42]E. K. Li, K. H. Johnson, D. E. Eastman, and J. L. Freeouf, Phys. Rev. Lett. 32, 470 (1974).
[43]J. A. Roth and C. R. Crowell, J. Vac. Sci. Technol. 15, 1317 (1978).
[44]P. S. Ho, H. Föll, J. E. Lewis, and P. E. Schmid, in *Proceedings of the Fourth International Conference on Solid Surfaces and The Third European Conference on Surface Science, 1980, Cannes, France,* edited by D. A. Degras, and M. Costa (Societe Française du Vide, Paris, 1980), Vol. 2, p. 1376.
[45]A. R. Williams, D. D. Gelatt, Jr., and V. L. Moruzzi, Phys. Rev. Lett. 44, 429 (1980).
[46]M. Salmerón, A. M. Baró, and J. M. Rojo, Phys. Rev. B 13, 4348 (1976).
[47]P. W. Palmberg, G. E. Riach, R. E. Weber, and N. C. MacDonald, *Handbook of Auger Electron Spectroscopy* (Physical Electronics Industries, Minnesota, 1972).
[48]H. Raether, in *Excitation of Plasmons and Interband Transitions by Electrons,* Vol. 88 of *Springer Tracts in Modern Physics,* edited by G. Höhler (Springer, Berlin, 1980), p. 15.
[49]B. Aronsson, T. Lundström, and S. Rundqvist, *Borides, Silicides and Phosphides* (Wiley, New York, 1965).
[50]H. J. Goldschmidt, *Interstitial Alloys* (Butterworths, London, 1967).
[51]L. Pauling and A. M. Soldate, Acta Crystallogr. 1, 212 (1948).